Polarization-insensitive medium-switchable holographic metasurfaces

Haogang Cai[†,*], James A. Dolan[†], George Gordon, Taerin Chung, and Daniel López[*]

Haogang Cai - *Tech4Health Institute and Department of Radiology, NYU Langone Health, New York, New York 10016, United States; Center for Nanoscale Materials, Argonne National Laboratory, Lemont, Illinois 60439, United States;* orcid.org/0000-0003-1700-2531

James A. Dolan - *Department of Chemistry, University of Cambridge, Lensfield Road, Cambridge CB2 1EW, United Kingdom; Pritzker School of Molecular Engineering, University of Chicago, Chicago, Illinois 60637, United States; Center for Molecular Engineering, Argonne National Laboratory, Lemont, IL 60439, United States;* orcid.org/0000-0001-5019-1544

George Gordon - *Department of Electrical and Electronic Engineering, University of Nottingham, University Park, Nottingham NG7 2RD, United Kingdom;* orcid.org/0000-0002-7333-5106

Taerin Chung - *Tech4Health Institute and Department of Radiology, NYU Langone Health, New York, New York 10016, United States;* orcid.org/0000-0001-5763-1207

Daniel López - *Electrical Engineering and Materials Research Institute, Millennium Science Complex, Penn State University, University Park, Pennsylvania 16802, United States;* orcid.org/0000-0001-7174-4013

[*] Email: haogang.cai@nyu.edu, dlopez@psu.edu. [†] These authors contributed equally.

Abstract

The adoption of metasurfaces has led to revolutionary advances in holography due to improved compactness, integrability, and performance. Switchable meta-holograms projecting different

replay field images in a controllable manner are highly desirable. Still, existing technologies generally rely on the use of polarized light and additional optics to facilitate switching. Consequently, the potential benefits afforded through the use of metasurfaces are limited both by the system complexity and a fixed relationship between the optical input and output. In this manuscript, we demonstrate polarization-insensitive metasurfaces encoding arbitrary and independent holograms, which can be switched between by changing the refractive index of the infiltration medium while maintaining identical illumination conditions. By sidestepping the requirements for high-performance light sources, switching optics, or delicate alignment, this approach points towards ultra-compact and cost-effective switchable meta-holograms for various practical applications, such as holographic image projection, eye-perceptible sensors, optical information storage, processing, and security.

Key words

Tunable metasurface, meta-hologram, all-dielectric, transmissive, visible spectrum, ultra-compact, cost-effective

Introduction

For decades, holography has been one of the most striking applications of optical wavefront engineering, due to holograms' ability to record and reconstruct both the amplitude and phase of incident light.[1] With the recent rise of metasurface technology, the use of metasurfaces to generate holograms—so called meta-holograms—has become an area of particular interest.[2] By providing smaller form factors, better performance (e.g., higher quality, better resolution, wider viewing angle, etc.), compatibility with semiconductor production processes, independent modulation of

both amplitude and phase,[3] meta-holograms promise a new generation of applications in augmented reality and wearable displays, optical information storage, processing, and security (e.g., encryption and anticounterfeiting).[4, 5] More importantly, dynamically switchable meta-holograms which respond to external stimuli will not only enhance the abovementioned holographic applications, but will also enable integrated visual reporting for sensing applications.[6]

Conventional metasurfaces—and, by extension, meta-holograms—are static and designed to work in only a single state: a specific device configuration with specific illumination conditions giving rise to a fixed relationship between the optical input and output. Subsequent modulation of any system parameters in an attempt to tune the response of such a metasurface will, in general, "switch off" the response due to a substantial deviation from the designed operational state. Although arguably a second state, the "off" state is extremely simple and rarely, alone, encodes any new or valuable information. In order to introduce multiple replay field images within a single meta-hologram, the most straightforward approach is spatial multiplexing (i.e., interleaving) of two different sets of single-state ("on/off") meta-atoms, which are selected between either by illumination conditions (Fig. 1a), such as polarization[7] and wavelength,[8, 9] or by metasurface actuation (Fig. 1b), such as chemical reaction.[10] An alternative approach combines multiplane holograms (i.e., holograms which project different images at different distances) with the isotropic stretching of a flexible metasurface, which leads to shifting/scaling of the replay fields and is equivalent to switching between distinct images at a specific imaging plane (Fig. 1c).[11] Overall, these single-state meta-atoms can only provide a single optical output, as shown by the inset flowcharts of Fig. 1a-c.

In order to expand the capacity of optical information storage and improve meta-holograms' performance for display and encryption applications, a non-interleaved design based on multi-state meta-atoms is required, where each meta-atom provides independent multiple outputs in corresponding states (i.e., two or more states, where neither state is the "off" state). So far, such non-interleaved multi-state metasurfaces are limited to switching via illumination modulation (Fig. 1d), where different optical outputs are encoded by light polarization,[12, 13] incident angle,[14] wavelength or spin.[6, 15-17] A large number of outputs have been demonstrated using complex light sources, such as a dynamic structured laser beam for spatially multiplexed metasurfaces,[18] and different orbital angular momentum modes for complex-amplitude metasurfaces.[19] However, additional optics are required to read out the information encoded in the response of static meta-atoms to a specific set of input illumination conditions (inset flowchart of Fig. 1d).

In this work, we implement multi-state meta-atoms in switchable meta-holograms by medium control (Fig. 1e, f). Often realized using liquid crystals (LCs) due to their optical anisotropy and response to external stimuli, changes in the surrounding medium can modulate the resonance,[20, 21] intensity,[22-24] phase,[25] and light emission of a metasurface.[26] In particular, phase modulation has been used for beam steering[27] and focusing,[28-30] either of which demands the implementation of two one-dimensional (linear or radial) phase profiles. These phase profiles will, in general, be correlated, often leading to switching behavior even if not explicitly designed for. Multi-state holography is a more demanding application, which requires the successful implementation of two two-dimensional phase profiles, each determined by an inverse Fourier transform, and which will, in general, bear little relation to one another.

Many conventional hologram encoding media have a strong polarization sensitivity.[31] Since most existing switchable meta-holograms and tunable LC metasurfaces rely on the interaction between polarized light and anisotropic meta-atoms (Fig. 1a-d) or LCs, respectively, they are similarly bound by this same intrinsic limitation and therefore only work with specifically polarized light. This inevitably leads to greater demands on the optics and assembly. Moreover, the most popular switchable multi-state meta-holograms rely on the switching of input illumination conditions (e.g., polarization, Fig. 1d), which requires additional bulky optical components. Therefore, the benefits afforded through the use of compact metasurfaces are limited by the system complexity. Efforts have been made to integrate a polarization conversion layer onto the back of the metasurface substrate,[6, 17] yet an initial polarized input is still required. Here, we demonstrate ultra-compact monolithic meta-holograms, which are polarization-insensitive and medium-switchable, therefore fundamentally eliminate the requirement of any polarizing or polarization conversion optics, as well as the need to ensure alignment to any specific polarization direction (Fig. 1f). As a non-interleaved design, each meta-atom provides distinct phase outputs (rather than the "on/off" of a single state), controlled by the infiltration medium under identical illumination conditions. This goes beyond existing fixed one-to-one relationships between the optical input and output. As a proof of concept, the switching between two independent holograms is implemented by switching the surrounding medium between air and water.

Results

Resonance tuning in Huygens' metasurfaces

In this work, we utilized Huygens' metasurfaces, consisting of arrays of high-refractive-index TiO_2 dielectric resonators as meta-atoms on a glass substrate.[32, 33] It is well known that such optical

resonators exhibit electric and magnetic resonances that can be engineered to manipulate light with negligible losses compared to equivalent plasmonic resonators.[34] Consider a cylindrical dielectric particle as a prototypical meta-atom—it exhibits an electric dipole (ED) and a magnetic dipole (MD) when illuminated along its axis of symmetry. By adjusting the geometric parameters of the resonator (e.g., its radius *r*), the backscattering emission by both dipoles can be adjusted to cancel out one another, leaving only forward transmission and negligible reflection, as articulated by the Huygens' principle.[35] From the finite-difference time-domain (FDTD) simulated spectra (Fig. 1e), it is clear that the spectral positions of the ED and MD resonances can be manipulated to merge the two resonances together. This provides both high transmission and phase modulation and is referred to as the Huygens' condition.[36] This concept has been widely used to create ultrathin metasurfaces—Huygens' metasurfaces—both to circumvent the fabrication of high-aspect-ratio waveguide-type nanostructures and to improve compatibly with standard semiconductor fabrication processes. Due to the limited availability of high-index lossless materials in the visible spectrum, most Huygens' metasurfaces demonstrated to-date work in wavelength ranges above that of visible light.[37, 38] Holographic Huygens' metasurfaces have therefore been demonstrated from telecommunication wavelengths down to near infrared using silicon.[31, 39, 40]

In the visible spectrum, TiO_2 exhibits a high refractive index and negligible loss, and has therefore been used in a large variety of waveguide-type metasurfaces.[7, 12, 13] Unlike such metasurfaces, which are composed of high-aspect-ratio phase-shifter elements that exhibit strong light confinement, Huygens' metasurfaces utilize thin resonators which are very sensitive to adjacent neighbors and the local dielectric environment. While the design of a Huygens' metasurface is more challenging due to these nonlocal interactions,[33, 41] their sensitivity to the local environment

is a distinct advantage when it comes to creating multi-state meta-atoms under identical illumination conditions. Here we demonstrate TiO_2 Huygens' meta-holograms in the visible spectrum with tunability controlled by the surrounding dielectric environment. Fig. 1e shows the working principle: the meta-atom resonances are tailored by the in-plane geometry to reproduce the desired phase modulation, which can be further tuned by the surrounding media to achieve multi-state optical responses. The constituent Huygens' resonators are cylindrical in shape, arranged in a homogeneous and periodic subarray, and are therefore polarization insensitive. The subarray will constitute a single pixel in the eventual meta-hologram.

To design the meta-holograms, we first used FDTD simulations to build a database of transmittance (T) and phase (Φ) values for light transmitted through the metasurfaces by varying the resonators' geometrical parameters and the refractive index of the surrounding medium—air ($n_1 = 1$, Fig. 2a) vs. water ($n_2 = 1.333$, Fig. 2b). The sub-arrays are modelled by a single nanodisc with periodic boundary conditions in the corresponding medium (insets of Fig. 2a,b), with geometric parameters including the thickness t and radius r of the discs, and the edge-to-edge gap g between discs. The thickness $t = 120$ nm was chosen to ensure that the Huygens' condition is met in a range of in-plane geometric parameters appropriate for robust nanofabrication. For a given wavelength of 532 nm, the transmittance and phase of the transmitted light are plotted for each parameter pair by sweeping the radius and gap along the x and y axes respectively. The low transmission bands indicate that the resonances reduce the transmitted light intensity at those specific geometric parameters, accompanied by significant phase modulation. The Huygens' condition is fulfilled when the ED and MD resonances merge together, providing both high transmission and a full 2π phase modulation (i.e., white circles in Fig. 2a,b). As expected, the

resonances—and therefore also the optical response (transmittance and phase)—are strongly influenced by the surrounding medium. When the medium is changed from air (Fig. 2a) to water (Fig. 2b), the low transmission bands become narrower and shift towards lower radius geometric parameter pairs. The change in optical response demonstrates how the resonance of each meta-atom array can be tuned by the medium, providing the necessary multi-state meta-atom library for tunable metasurface design.

In Fig. 2c,d, we show the experimentally measured transmittance of the meta-atom library simulated in Fig. 2a,b, derived from optical microscope images under unpolarized green light (532 nm, filtered light from a Halogen lamp). The meta-atoms were fabricated using a high-precision process, whereby the thickness was controlled by atomic layer deposition (ALD) and the in-plane geometry was patterned by a single electron beam lithography step, followed by lift off and reactive ion etching (Fig. S1).[33] This fabrication process is fully compatible with standard semiconductor manufacturing, thanks to the low-aspect-ratio structures. We fabricated super-arrays (i.e., an "array of arrays") where each pixel (dimensions 5x5 μm^2) is a subarray of TiO_2 nanoresonators with constant radius and gap, schematically shown in the insets of Fig. 2c,d. Between different subarrays, the radius of the nanodiscs and the gap between them are incrementally increased along the x and y axes respectively, similar to the parameter sweep plots in our optical simulations. The superarray exhibits resonance patterns, both in air (Fig. 2c) and water (Fig. 2d), in good agreement with simulations (Fig. 2a,b). The measured and simulated transmittance values differ at large values of radius and gap (pitch $2r + g > \lambda$) due to diffraction—i.e., the periodicity of the metasurface is such that some light is diffracted at angles not captured by the finite numerical aperture of the microscope objective lens but still captured by the simulated

transmission monitor (see ref. [21] for more details). The meta-atoms affected by diffraction are excluded from the library for meta-hologram design.

Meta-hologram design algorithms: single vs. multi-state

Once the meta-atom library was experimentally verified by fabrication and characterization of the metasurface superarrays, it was imported to the holographic metasurface design algorithm (Fig. 3). Assuming first a single-state design (Fig. 3a), the ideal phase mask $\Phi_1^i(x,y)$ (i.e., a phase-only, constant-amplitude hologram) that would result in the desired (target) replay field $I_1^t(x,y)$ was computed using the Gerchberg-Saxton (G-S) algorithm[1]. For each pixel (x,y), the meta-atom library $\tilde{T}_1^l(r,g)$ (Fig. 2a) was searched to identify the specific metasurface geometric parameters (r, g) which give rise, in n_1 (air), to a metasurface optical response $\tilde{T}^m(r,g)$ closest to the ideal value $e^{j\Phi_1^i(x,y)}$ (i.e., a transmittance of 100% and a phase of $\Phi_1^i(x,y)$). This optimal geometric parameter pair (r^*,g^*) was assigned to the corresponding pixel (x,y) of the meta-hologram. In this way, appropriate meta-atom subarrays were placed in the overall metasurface layout $r^*(x,y)$ and $g^*(x,y)$ to reproduce, as closely as possible, the ideal phase mask. The resulting metasurface hologram $\tilde{T}_1^m(x,y)$ could be used to simulate the associated replay field $I_1^m(x,y)$. In the example shown in Fig. 3a, a target image (the letter "A") is well-reproduced by the simulated single-state meta-hologram. If that same single-state meta-hologram were to be placed in water, a surrounding medium for which it was not designed, the simulation indicates that the replay field image has much lower intensity (i.e., it "turns off", as indicated in the dashed rectangle in Fig. 3a). Fig. S2a shows the results of the corresponding experiment, which is in excellent agreement with the simulated results: a single-state meta-hologram designed in the manner of Fig. 3a correctly projects the letter "A" in the replay field, and upon change in the surrounding medium from air to water,

the output image significantly lowers in intensity (i.e., the image is almost entirely turned "off"). Fig. S3a shows, as a function of the geometric parameter space, the subset of meta-atoms selected for the meta-hologram in Fig. 3a. As we use a phase-only G-S algorithm for the hologram design, the selected metasurface parameter pairs avoid the low transmission bands and makes full use of the available phase shifts. For this single-state design, when the surrounding dielectric medium is changed from air to water, the meta-atom selection in air no longer corresponds to the ideal hologram, and some selected parameter pairs now reside in low transmission regions of the parameter space. As a result, the efficiency is considerably lower (compare the phase masks of letter "A" in air vs. water in Fig. 3a). In other words, simply changing the surrounding dielectric medium of a single-state meta-hologram results only in performance degradation, similar to other switchable metasurface devices when designed according to the optical properties corresponding to only a single state.[28]

In order to create a tunable multi-state meta-hologram, which projects an independent replay field in each state, we developed a design strategy as illustrated in Fig. 3b (two-state as an example). Starting from two different target images $I_1^t(x,y)$ and $I_2^t(x,y)$ for n_1 (air) and n_2 (water), two ideal phase masks $\Phi_1^i(x,y)$ and $\Phi_2^i(x,y)$ were computed using the G-S algorithm, respectively. It is critical to then search the meta-atom libraries $\tilde{T}_1^l(r,g)$ and $\tilde{T}_2^l(r,g)$ so that the two ideal complex transmittances $e^{j\Phi_1^i(x,y)}$ and $e^{j\Phi_2^i(x,y)}$ are simultaneously achieved, as far as possible, in the respective states. The metasurface complex transmittances, incorporating both the amplitude and phase information of metasurfaces in two different media, $\tilde{T}_1^l(r,g)$ and $\tilde{T}_2^l(r,g)$ (Fig. 2a,b), were fed into the multiplexing algorithm (library search), together with the two target phase masks. For each pixel, at a given position (x, y), the geometric parameters (r, g) were selected to minimize

the mean square error between the ideal (G-S) complex transmittances in both states and what could be achieved by searching the meta-atom library. In this way, an optimal meta-hologram layout (r^*, g^*) was designed to realize two different phase masks, $\tilde{T}_1^m(x,y)$ and $\tilde{T}_2^m(x,y)$—and, by extension, two different replay fields, $I_1^m(x,y)$ and $I_2^m(x,y)$—by switching the meta-atom surrounding dielectric medium. In Fig. 3b, the target images of a letter "A" (representing a medium of air) and "W" (representing a medium of water) are clearly identifiable in the simulated replay fields, corresponding to distinct phase masks in air and water, respectively. The experimental results of the design outlined in Fig. 3b are shown in Fig. S2b and show excellent agreement. Notably, the meta-atom selection for the two-state design ("A" in air and "W" in water, Fig. S3b) is significantly different from that of the single-state design ("A" in air only, Fig. S3a), avoiding the low transmission bands and making use of the phase change in both two states, highlighting the distinct behavior of the multi-state design strategy.

Polarization-insensitive switchable meta-holograms

Switchable two-state meta-holograms were fabricated following the same process as the abovementioned superarrays. To demonstrate the versatility of encoding arbitrary and independent holograms, various combinations of images were used in the experiments. For example, one meta-hologram was designed to project a New York University (NYU) torch in air and an Argonne National Laboratory logo in water (Fig. 4a). Fig. 4b shows the SEM images of the fabricated pixelated holographic metasurfaces. The radius and gap of the resonator subarray in each pixel (dimensions 5x5 μm^2) were determined by the strategy described above (Fig. 3b). The fabricated meta-holograms were imaged in a 2-f system, with a chamber that allows the infiltration and removal of water to and from the metasurface (Fig. 4c, Fig. S4a). The fabricated meta-holograms

successfully generated replay fields which were in excellent agreement with simulations (Fig. 4d). The hologram efficiencies in air and water were 26.9% and 10.8% respectively, which are lower than the simulated 39% and 16% probably due to nanofabrication and material imperfection. The crosstalk between the two states, i.e., spatial overlapping of the two images, is minimal. The crosstalk and theoretical efficiency limit are caused by the incomplete coverage of the (Φ_1, Φ_2) phase space (as shown in Fig. S3c). The phase values provided by the meta-atom library in two states are not completely independent to each other, i.e., for some phase values in one state, there is only a limited range of available phase values in the second state and a full 2π phase modulation is not always possible.

Another example was designed to project a NYU torch in air and both an Argonne logo and Center for Molecular Engineering (CME) logo in water (Fig. 5). Instead of a linearly polarized diode-pumped solid-state (DPSS) laser, as used in the previous experiment, we used an unpolarized diode laser pointer to demonstrate the robustness of the design to the use of a more compact and cost-effective light source (Fig. S4b). Furthermore, the laser pointer is linearly polarized in different directions to verify the polarization insensitivity (Fig. S4c). The designed replay fields were all successfully generated and switched in agreement with simulations, irrespective of the polarization state of the incident light from the laser pointer, whether unpolarized or linearly polarized in different directions: 0°, 45°, 90°. No significant difference was observed in these images, while the exposure time under unpolarized light is half of that under linearly polarized light. This demonstrates another advantage of polarization insensitivity: lower power consumption when there is no need to polarize incident unpolarized light. Thanks to its robustness to various illumination conditions, the switchable meta-hologram can be integrated with miniaturized low-

cost light sources, such as a diode laser, without any additional optics or delicate alignment.

In addition to the experimental demonstration of switchable two-state meta-holograms, we also perform simulations to demonstrate that our design strategy can be expanded to multi-state holograms with more than two states. Fig. S5 shows a simulated switchable three-state meta-holograms including air, water, and a third medium with a higher refractive index of $n_3 = 1.398$, which can be implemented using 40% glucose or 50% glycerine solutions (by weight). Moreover, with this expanded three-state meta-atom library, we are also able to inspect the two-state hologram replay fields at a third state different from the designed two states. Fig. S6a-c show the simulations when the medium refractive index is larger, intermediate, or smaller than the designed two states respectively, all resulting in reduced efficiency and increased crosstalk. As expected, the hologram quality is optimized at the designed states. Notably, n_2 and n_3 are closer to each other than n_1, leading to a higher correlation between phase values in these two states (Fig. S5a). As a result, the crosstalk between n_2 and n_3 are more significant among various two-state (Fig. S6) and three-state (Fig. S5b) designs.

Discussion

This work demonstrates the first polarization-insensitive switchable meta-hologram. The projection of arbitrary and independent replay fields can be switched by the on-chip surrounding medium (Fig. 1f). This is in contrast to existing switchable meta-holograms that rely on polarized light and illumination modulation, such as polarization switching (Fig. 1a-d). By sidestepping the requirements for high-performance light sources, bulky optics, delicate alignment or individually addressed pixels, it provides a practical solution for reversible switching between pre-encoded

states of interest for situations where a large number of sates or dynamic “reprogramming” is not needed. This constitutes by far the simplest implementation among all switching strategies (comparing the inset flowcharts of Fig. 1f vs. Fig. 1a-d), and therefore better facilities the small form factor and low cost promised by metasurfaces. Allowing the integration with miniaturized light source (e.g., diode laser), it points to practical ultra-compact and wearable applications (e.g., on safety goggles or eyewear), such as hologram projection and eye-perceptible sensors.

As a non-interleaved design, each meta-atom provides distinct phase outputs under identical illumination condition (Fig. 1f), which overcomes the limitation of a fixed relationship between the optical input and output (Fig.1a-d) and thereby adds an extra degree of freedom to dynamic tunable meta-hologram design. The combination of different switching approaches (e.g., spin and wavelength) could greatly increase the number of holograms generated on a single metasurface.[16] Similarly, the additional degree of freedom offered by medium tuning could also be incorporated into existing light modulation approaches, therefore enabling novel designs with more complex tunable functions and expanded capabilities for optical information storage, processing, and security. For example, the combination of medium and wavelength switching was recently demonstrated, resulting in colorful holographic mimicry on metallic reflective metasurfaces for near infrared.[42] Our all-dielectric transmissive metasurfaces offer the potential for a similar combination for visible light.

In this work, the surrounding medium was switched, as a proof of concept, between air and water. The liquid infiltration could, in the future, be implemented by integrating a microfluidic channel (e.g., made of PDMS) on top of the metasurface.[22] To further simplify and optimize the liquid

injection and ejection processes, electro-wetting could be used to control the liquid coverage on metasurfaces by external electrical switching with microsecond-scale response times.[43] We envision many more possibilities, however, when using functional materials other than water as the meta-atoms' dielectric environment.[21] For example, a refractive index change in response to external stimuli (thermal, electrical, chemical, etc.) would not only enable ultracompact sensors integrated with holographic visual reporting,[6] but would also expand our multi-state design strategy to achieve an increased number of states in response to increasingly fine changes of the refractive index (Fig. S5). Here, the nonlocal interactions between ultrathin Huygens' resonators[41] were circumvented by using a pixelated layout, where each pixel (dimensions 5x5 μm^2) is a homogeneous subarray of resonators with identical geometric parameters. In order to take full advantage of metasurfaces' promise of sub-wavelength-scale pixels for improved hologram performance, the pixel size should be reduced by taking into account the nonlocal interactions among adjacent meta-atoms. This can be done using our recently developed inverse design strategies.[33] Finally, other computational methods could be used to minimize the crosstalk and improve the hologram efficiency, by better fulfilling the multiple states simultaneously. For example, we are developing a gradient descent-type algorithm to directly optimize the replay fields with the available meta-atom library. The morphology of the meta-atoms can be designed to maximize the phase value coverage in (Φ_1, Φ_2) space, where a circular symmetry could be used to maintain the polarization insensitivity.[44]

Methods

FDTD Simulation

A commercial FDTD software (Lumerical) was used for nanoresonator and metasurface simulations. To build a library of metasurface optical responses, a uniform TiO_2 nanoresonator array was simulated by modelling a single nanodisc with periodic boundary conditions in both the *x* and *y* in-plane directions. The light transmittance was quantified as the power transmitted through the nanoarray, normalized to the source power. The Huygens' resonator spectra were simulated (t = 115 nm, g = 36 nm) for various disc radius r and medium refractive index n, as outlined in Fig. 1e. The switchable meta-hologram design was based on a multi-state meta-atom library (t = 120 nm), whose geometric parameters of both radius r and gap g were swept according to the parameter space outlined in Fig. 2, in surrounding media of both air and water.

Nanofabrication

The metasurfaces were composed of TiO_2 nanoresonators, whose thickness was precisely controlled by atomic layer deposition (ALD), and the in-plane geometry was patterned by electron beam (e-beam) lithography, which is shown schematically in Fig. S1. Glass substrates with 115 nm thick TiO_2 ALD-deposited film were spin-coated with a bilayer of e-beam resist polymethyl methacrylate (PMMA), and then sputtered with 10 nm Au as a conductive layer. The samples were patterned by a single e-beam lithography step. After exposure, the Au conductive layer was removed by wet etching. The samples were developed in (methyl isobutyl ketone) MIBK/isopropanol (IPA) 3:1 at 4 °C with ultrasonication for 1 min. A 10 nm Cr layer was deposited by e-beam evaporation and then lift off, forming hard masks for pattern transfer. After dry etching of TiO_2 and wet etching of the Cr mask, metasurfaces of TiO_2 nanoresonator arrays were formed on the glass substrates.

Optical characterization

An inverted microscope (Olympus IX73) was used to image the superarrays in transmission (Fig. 2c,d). The white light from Halogen lamp was filtered by 532 nm band-pass filters with 10 nm bandwidth (Edmund Optics). The meta-holograms were imaged using a DPSS laser (532 nm, Opto Engine) in a 2-f system (Fig. 4c, Fig. S4a). Alternatively, a 532 nm diode laser pointer was used for the imaging under unpolarized light (Fig. S4b). An additional film polarizer and half-waveplate were used to adjust the polarization directions (Fig. S4c). Note that the polarizing optics were only used to verify the polarization-insensitivity, and will not be needed in practical applications, which is a major advantage compared with existing switching strategies. A glass coverslip is attached on top of the metasurface sample to form a chamber for medium switching (e.g., infiltration and removal of de-ionized water). The imaging after infiltration or removal of water was repeated multiple times without any difference.

Acknowledgements

This work was performed, in part, at the Center for Nanoscale Materials, a U.S. Department of Energy Office of Science User Facility, and supported by the U.S. Department of Energy, Office of Science, under Contract No. DE-AC02-06CH11357. The authors gratefully acknowledge the ongoing technical support of Dr. David A. Czaplewski.

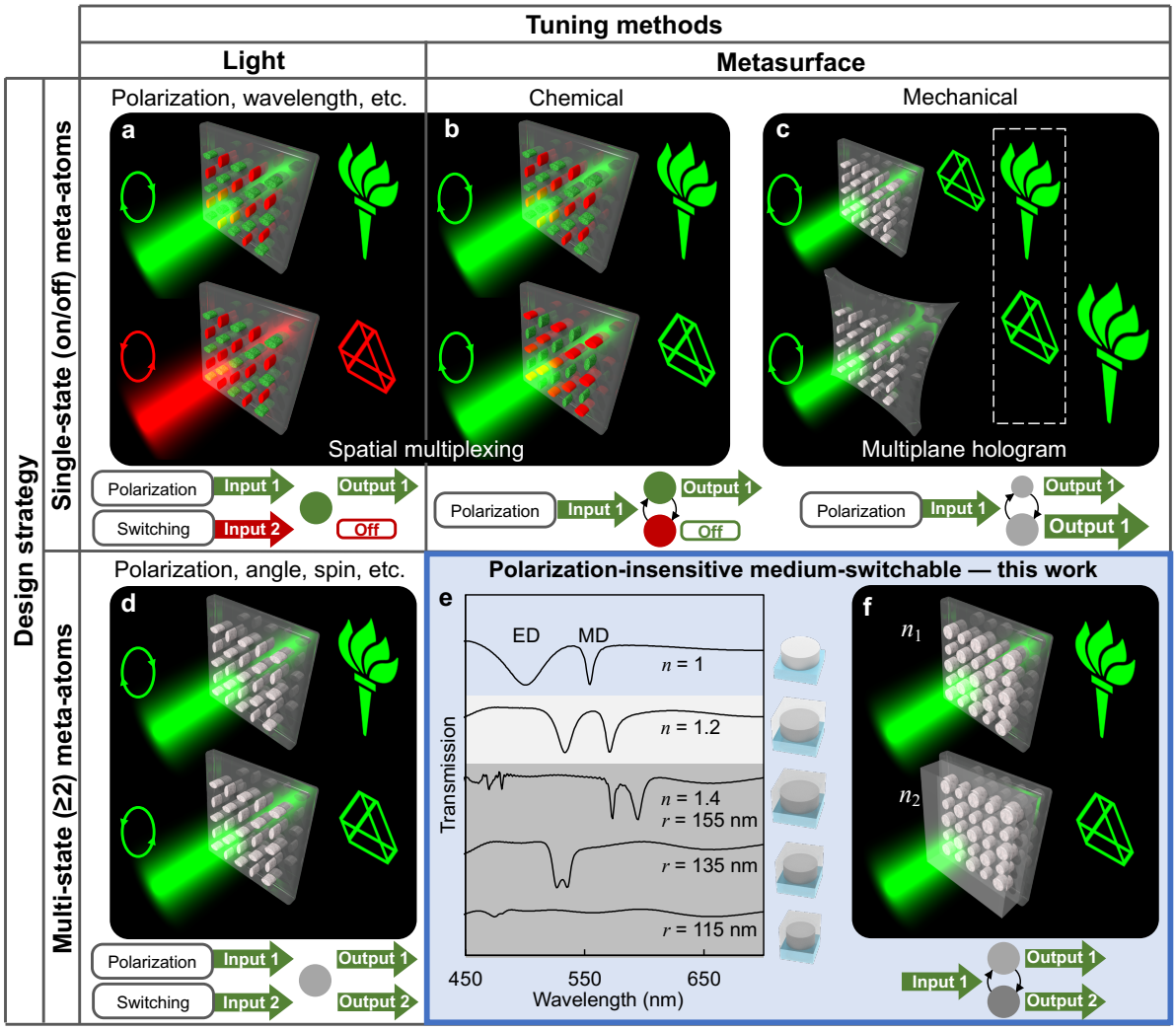

Fig. 1 Switchable meta-holograms: existing technologies vs. polarization-insensitive medium-switching. Meta-holograms may be tuned by modulation of either the incident light or the metasurface, which could be composed of either single-state (i.e., "on/off") or multi-state meta-atoms. (a) Two sets of single-state meta-atoms (red and green), each of which is responsive to a particular illumination condition (e.g., polarization, wavelength, etc.), spatially-multiplexed on a single metasurface, may be used to select independent replay fields via modulation of the incident light. (b) Two sets of single-state, spatially-multiplexed meta-atoms may similarly be used to select independent replay fields via reversible chemical reaction of the metasurface which inverts the on/off states of the two sets. (c) Alternatively, a set of single-state meta-atoms which encode a

multiplane hologram (projecting different images at different planes in the replay field) may, through isotropic stretching of the metasurface, select between multiple images at a specific imaging plane. (d) A single set of static multi-state meta-atoms may encode multiple holograms, selected between by light polarization, angle, wavelength and spin. (e) The optical resonances of Huygens' metasurfaces (the electric dipole, ED, and the magnetic dipole, MD) may be tuned as the refractive index n of the surrounding medium is varied. (f) Through careful design, a single set of multi-state meta-atoms may encode multiple independent replay fields, selected between via the surrounding medium (refractive indices n_1 and n_2) without the need for light modulation. The inset flowcharts schematically show that design (f) features isotropic meta-atoms and simplest system configuration, compared to anisotropic meta-atoms and additional optics in designs (a-d). The Argonne logo is used with permission from Argonne National Laboratory.

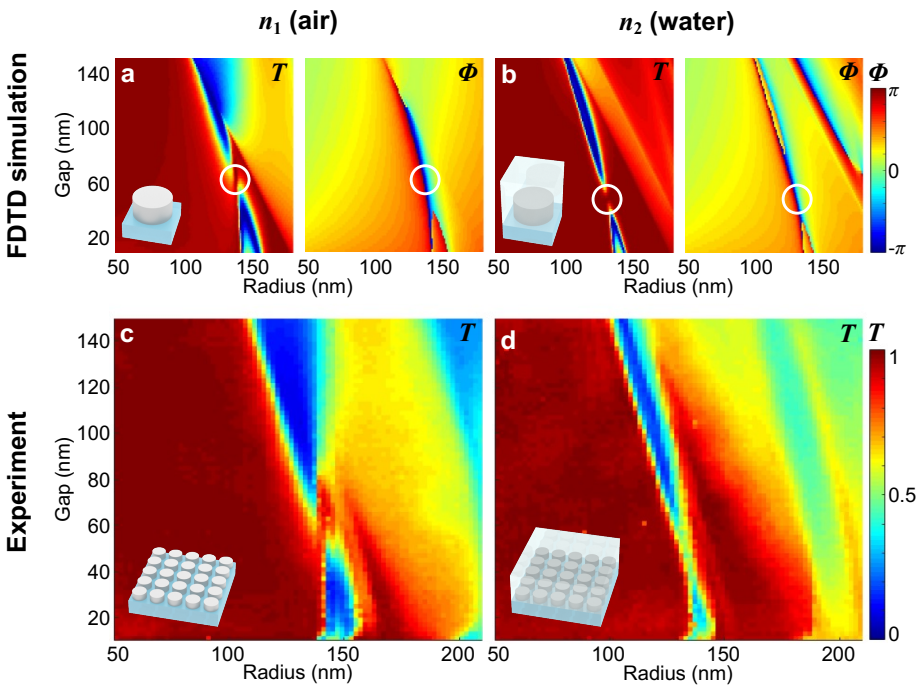

Fig. 2 Huygens' metasurfaces tuned by surrounding medium. FDTD simulation results of the transmittance (T) and phase shift (Φ) experienced by a uniform wavefront of light at 532 nm after propagation through a homogeneous and periodic TiO_2 nanoresonator array (modelled by a single nanodisc with periodic boundary conditions as shown in the inset) as a function of the resonator geometric parameters, disc radius r and edge-to-edge gap g, in surrounding medium of (a) air and (b) water. Experimental results measured by optical microscopy of the transmittance (T) though a metasurface superarray (i.e., an array of various subarrays with specific geometric parameters as shown in the inset) under filtered light (532 nm, unpolarized) in surrounding medium of (c) air and (d) water.

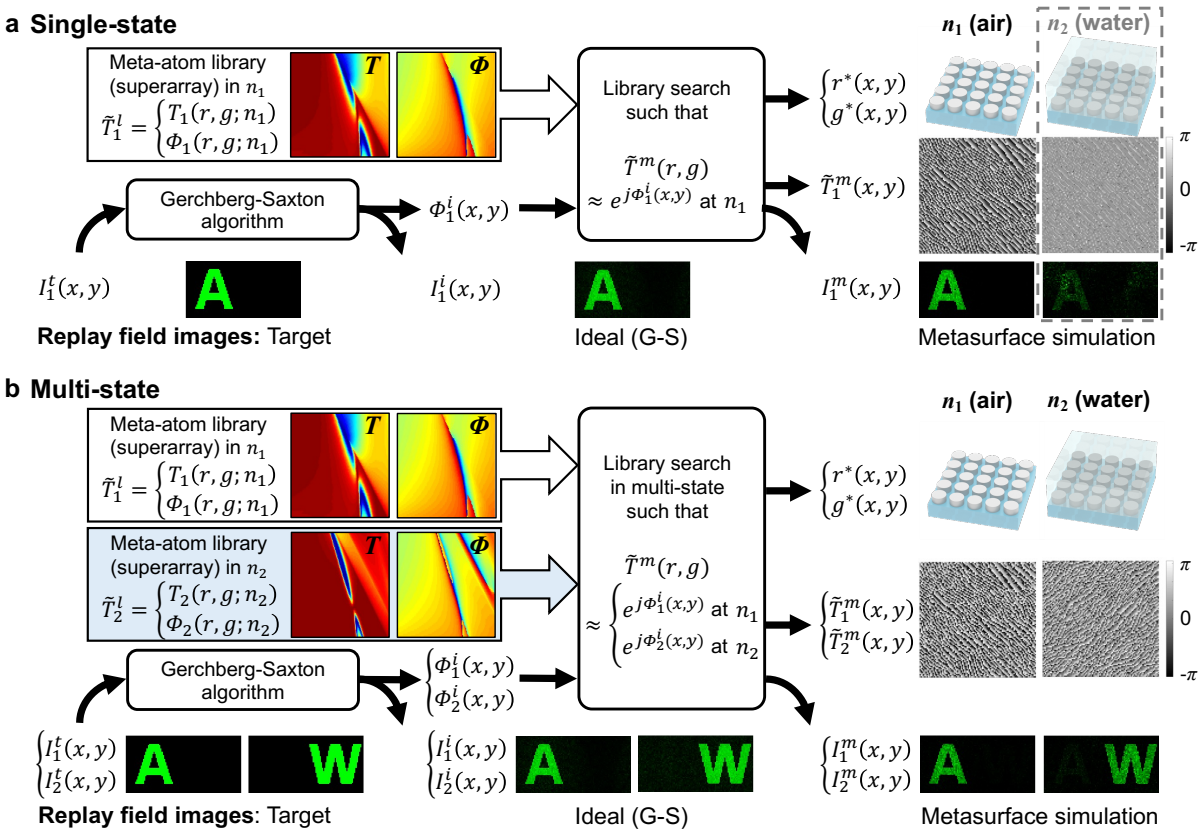

Fig. 3 Meta-hologram design algorithms. (a) Single-state vs. (b) multi-state. Target replay field images $I_1^t(x,y)$ and $I_2^t(x,y)$ are used to create ideal phase masks $\Phi_1^i(x,y)$ and $\Phi_2^i(x,y)$ via the Gerchberg-Saxton (G-S) algorithm, which generate ideal (G-S) replay field images $I_1^i(x,y)$ and $I_2^i(x,y)$. Library searches of the meta-atom libraries $\tilde{T}_1^l(r,g)$ and $\tilde{T}_2^l(r,g)$ to select optimal metasurface geometric parameters (r^*, g^*) for each pixel (x,y) yield meta-holograms $\tilde{T}_1^m(y,x)$ and $\tilde{T}_2^m(x,y)$ and the corresponding simulated meta-hologram replay fields $I_1^m(x,y)$ and $I_2^m(x,y)$. Subscripts refer to two states and the corresponding refractive indices of surrounding media, n_1 and n_2.

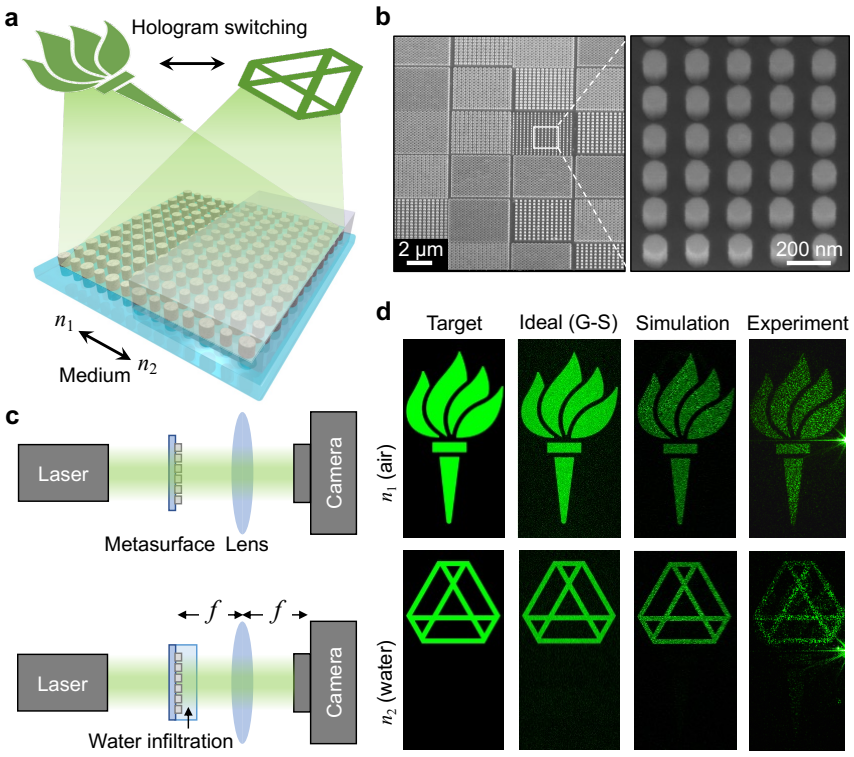

Fig. 4 Switchable meta-holograms controlled by the infiltration medium. (a) Schematic diagram of the medium-switching mechanism. (b) SEM images of the fabricated holographic metasurfaces, where the radius and gap of the homogeneous resonator array in each pixel (dimensions 5x5 μm^2) is determined by the strategy outlined in Fig. 3b. (c) Schematic diagram of the optical setup in air (top) and water (bottom), without any optics for illumination modulation. (d) Target images and replay fields including: ideal replay fields associated with the phase masks generated by the Gerchberg-Saxton algorithm; simulated replay fields corresponding to the optimally designed meta-hologram based on the meta-atom library; and experimental images of the meta-hologram replay fields in air (top: NYU torch) and water (bottom: Argonne logo, used with permission from Argonne National Laboratory).

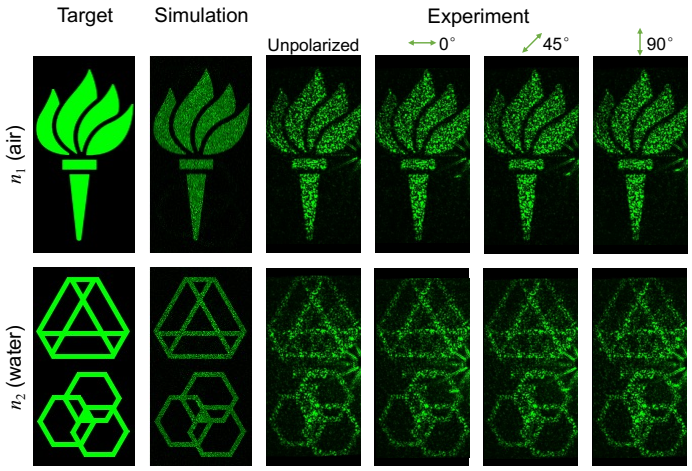

Fig. 5 Polarization insensitivity of the medium-switchable meta-holograms. Target images and replay fields including: simulated replay fields corresponding to the optimally designed meta-hologram based on the meta-atom library; and experimental images of the meta-hologram replay fields for unpolarized and linearly polarized light in different directions: 0°, 45°, 90°, both in air (top: NYU torch) and water (bottom: Argonne and CME logos, used with permission from Argonne National Laboratory).

For Table of Contents Use Only

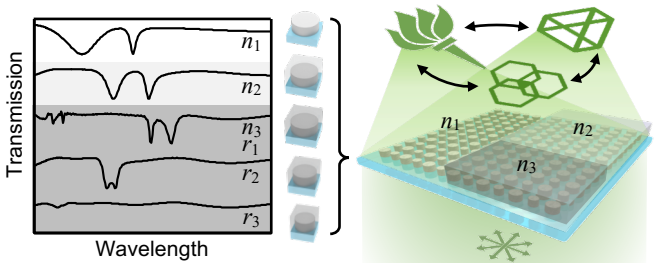

Polarization-insensitive medium-switchable holographic metasurfaces

Haogang Cai, James A. Dolan, George Gordon, Taerin Chung, and Daniel López

We demonstrate polarization-insensitive metasurfaces encoding arbitrary and independent holograms, which can be switched between by changing the refractive index of the infiltration medium while maintaining identical illumination conditions (even unpolarized light). Composed of TiO_2 cylindrical meta-atoms on glass substrate, the metasurfaces are all-dielectric, transmissive, polarization insensitive, and work for the visible light. The meta-atom resonances are tailored by the in-plane geometry to reproduce the desired phase modulation, which are further tuned by the surrounding media to achieve multi-state switching.

References

1. Goodman, J. W., *Introduction to Fourier optics*. Fourth edition. ed.; W.H. Freeman, Macmillan Learning: New York, 2017; p xiv, 546 pages.
2. Zheng, G.; Mühlenbernd, H.; Kenney, M.; Li, G.; Zentgraf, T.; Zhang, S., Metasurface holograms reaching 80% efficiency. *Nat Nanotechnol* **2015,** *10* (4), 308-312.
3. Lee, G.-Y.; Yoon, G.; Lee, S.-Y.; Yun, H.; Cho, J.; Lee, K.; Kim, H.; Rho, J.; Lee, B., Complete amplitude and phase control of light using broadband holographic metasurfaces. *Nanoscale* **2018,** *10* (9), 4237-4245.
4. Jiang, Q.; Jin, G.; Cao, L., When metasurface meets hologram: principle and advances. *Adv Opt Photonics* **2019,** *11* (3), 518-576.
5. Kim, I.; Yoon, G.; Jang, J.; Genevet, P.; Nam, K. T.; Rho, J., Outfitting Next Generation Displays with Optical Metasurfaces. *Acs Photonics* **2018,** *5* (10), 3876-3895.
6. Kim, I.; Kim, W.-S.; Kim, K.; Ansari, M. A.; Mehmood, M. Q.; Badloe, T.; Kim, Y.; Gwak, J.; Lee, H.; Kim, Y.-K.; Rho, J., Holographic metasurface gas sensors for instantaneous visual alarms. *Science Advances* **2021,** *7* (15), eabe9943.
7. Khorasaninejad, M.; Ambrosio, A.; Kanhaiya, P.; Capasso, F., Broadband and chiral binary dielectric meta-holograms. *Science Advances* **2016,** *2* (5).
8. Wang, B.; Dong, F. L.; Li, Q. T.; Yang, D.; Sun, C. W.; Chen, J. J.; Song, Z. W.; Xu, L. H.; Chu, W. G.; Xiao, Y. F.; Gong, Q. H.; Li, Y., Visible-Frequency Dielectric Metasurfaces for Multiwavelength Achromatic and Highly Dispersive Holograms. *Nano Lett* **2016,** *16* (8), 5235-5240.
9. Wei, Q.; Sain, B.; Wang, Y.; Reineke, B.; Li, X.; Huang, L.; Zentgraf, T., Simultaneous Spectral and Spatial Modulation for Color Printing and Holography Using All-Dielectric Metasurfaces. *Nano Lett* **2019**.
10. Li, J. X.; Kamin, S.; Zheng, G. X.; Neubrech, F.; Zhang, S.; Liu, N., Addressable metasurfaces for dynamic holography and optical information encryption. *Science Advances* **2018,** *4* (6).
11. Malek, S. C.; Ee, H.-S.; Agarwal, R., Strain Multiplexed Metasurface Holograms on a Stretchable Substrate. *Nano Lett* **2017,** *17* (6), 3641-3645.
12. Chen, W. T.; Yang, K. Y.; Wang, C. M.; Huang, Y. W.; Sun, G.; Chiang, I. D.; Liao, C. Y.; Hsu, W. L.; Lin, H. T.; Sun, S.; Zhou, L.; Liu, A. Q.; Tsai, D. P., High-Efficiency Broadband Meta-Hologram with Polarization-Controlled Dual Images. *Nano Lett* **2014,** *14* (1), 225-230.
13. Mueller, J. P. B.; Rubin, N. A.; Devlin, R. C.; Groever, B.; Capasso, F., Metasurface Polarization Optics: Independent Phase Control of Arbitrary Orthogonal States of Polarization. *Phys Rev Lett* **2017,** *118* (11).
14. Kamali, S. M.; Arbabi, E.; Arbabi, A.; Horie, Y.; Faraji-Dana, M.; Faraon, A., Angle-Multiplexed Metasurfaces: Encoding Independent Wavefronts in a Single Metasurface under Different Illumination Angles. *Physical Review X* **2017,** *7* (4).
15. Ye, W.; Zeuner, F.; Li, X.; Reineke, B.; He, S.; Qiu, C.-W.; Liu, J.; Wang, Y.; Zhang, S.; Zentgraf, T., Spin and wavelength multiplexed nonlinear metasurface holography. *Nat Commun* **2016,** *7* (1), 11930.
16. Jin, L.; Dong, Z.; Mei, S.; Yu, Y. F.; Wei, Z.; Pan, Z.; Rezaei, S. D.; Li, X.; Kuznetsov, A. I.; Kivshar, Y. S.; Yang, J. K. W.; Qiu, C.-W., Noninterleaved Metasurface for (26-1) Spin- and Wavelength-Encoded Holograms. *Nano Lett* **2018,** *18* (12), 8016-8024.

17. Kim, I.; Ansari, M. A.; Mehmood, M. Q.; Kim, W. S.; Jang, J.; Zubair, M.; Kim, Y. K.; Rho, J., Stimuli‐Responsive Dynamic Metaholographic Displays with Designer Liquid Crystal Modulators. *Adv Mater* **2020**, 2004664.
18. Gao, H.; Wang, Y.; Fan, X.; Jiao, B.; Li, T.; Shang, C.; Zeng, C.; Deng, L.; Xiong, W.; Xia, J.; Hong, M., Dynamic 3D meta-holography in visible range with large frame number and high frame rate. *Science Advances* **2020,** *6* (28), eaba8595.
19. Ren, H.; Fang, X.; Jang, J.; Bürger, J.; Rho, J.; Maier, S. A., Complex-amplitude metasurface-based orbital angular momentum holography in momentum space. *Nat Nanotechnol* **2020**.
20. Komar, A.; Fang, Z.; Bohn, J.; Sautter, J.; Decker, M.; Miroshnichenko, A.; Pertsch, T.; Brener, I.; Kivshar, Y. S.; Staude, I.; Neshev, D. N., Electrically tunable all-dielectric optical metasurfaces based on liquid crystals. *Appl Phys Lett* **2017,** *110* (7).
21. Dolan, J. A.; Cai, H.; Delalande, L.; Li, X.; Martinson, A. B. F.; de Pablo, J. J.; López, D.; Nealey, P. F., Broadband Liquid Crystal Tunable Metasurfaces in the Visible: Liquid Crystal Inhomogeneities Across the Metasurface Parameter Space. *Acs Photonics* **2021,** *8* (2), 567-575.
22. Sun, S.; Yang, W.; Zhang, C.; Jing, J.; Gao, Y.; Yu, X.; Song, Q.; Xiao, S., Real-Time Tunable Colors from Microfluidic Reconfigurable All-Dielectric Metasurfaces. *Acs Nano* **2018,** *12* (3), 2151-2159.
23. Zou, C.; Komar, A.; Fasold, S.; Bohn, J.; Muravsky, A. A.; Murauski, A. A.; Pertsch, T.; Neshev, D. N.; Staude, I., Electrically Tunable Transparent Displays for Visible Light Based on Dielectric Metasurfaces. *Acs Photonics* **2019,** *6* (6), 1533-1540.
24. Li, J.; Yu, P.; Zhang, S.; Liu, N., Electrically-controlled digital metasurface device for light projection displays. *Nat Commun* **2020,** *11* (1).
25. Li, S. Q.; Xu, X.; Maruthiyodan Veetil, R.; Valuckas, V.; Paniagua-Dominguez, R.; Kuznetsov, A. I., Phase-only transmissive spatial light modulator based on tunable dielectric metasurface. *Science* **2019,** *364* (6445), 1087-1090.
26. Bohn, J.; Bucher, T.; Chong, K. E.; Komar, A.; Choi, D. Y.; Neshev, D. N.; Kivshar, Y. S.; Pertsch, T.; Staude, I., Active Tuning of Spontaneous Emission by Mie-Resonant Dielectric Metasurfaces. *Nano Lett* **2018,** *18* (6), 3461-3465.
27. Komar, A.; Paniagua-Domínguez, R.; Miroshnichenko, A.; Yu, Y. F.; Kivshar, Y. S.; Kuznetsov, A. I.; Neshev, D., Dynamic Beam Switching by Liquid Crystal Tunable Dielectric Metasurfaces. *Acs Photonics* **2018,** *5* (5), 1742-1748.
28. Zhong, J.; An, N.; Yi, N.; Zhu, M.; Song, Q.; Xiao, S., Broadband and Tunable-Focus Flat Lens with Dielectric Metasurface. *Plasmonics* **2016,** *11* (2), 537-541.
29. Lininger, A.; Zhu, A. Y.; Park, J.-S.; Palermo, G.; Chatterjee, S.; Boyd, J.; Capasso, F.; Strangi, G., Optical properties of metasurfaces infiltrated with liquid crystals. *Proceedings of the National Academy of Sciences* **2020**, 202006336.
30. Bosch, M.; Shcherbakov, M. R.; Won, K.; Lee, H.-S.; Kim, Y.; Shvets, G., Electrically Actuated Varifocal Lens Based on Liquid-Crystal-Embedded Dielectric Metasurfaces. *Nano Lett* **2021**.
31. Chong, K. E.; Wang, L.; Staude, I.; James, A. R.; Dominguez, J.; Liu, S.; Subramania, G. S.; Decker, M.; Neshev, D. N.; Brener, I.; Kivshar, Y. S., Efficient Polarization-Insensitive Complex Wavefront Control Using Huygens' Metasurfaces Based on Dielectric Resonant Meta-atoms. *Acs Photonics* **2016,** *3* (4), 514-519.

32. Cai, H.; Czaplewski, D.; Ogando, K.; Martinson, A.; Gosztola, D.; Stan, L.; López, D., Ultrathin transmissive metasurfaces for multi-wavelength optics in the visible. *Appl Phys Lett* **2019,** *114* (7), 071106.
33. Cai, H.; Srinivasan, S.; Czaplewski, D. A.; Martinson, A. B. F.; Gosztola, D. J.; Stan, L.; Loeffler, T.; Sankaranarayanan, S. K. R. S.; López, D., Inverse design of metasurfaces with non-local interactions. *npj Computational Materials* **2020,** *6* (1).
34. Kuznetsov, A. I.; Miroshnichenko, A. E.; Brongersma, M. L.; Kivshar, Y. S.; Luk'yanchuk, B., Optically resonant dielectric nanostructures. *Science* **2016,** *354* (6314), 2472.
35. Decker, M.; Staude, I.; Falkner, M.; Dominguez, J.; Neshev, D. N.; Brener, I.; Pertsch, T.; Kivshar, Y. S., High-Efficiency Dielectric Huygens' Surfaces. *Adv Opt Mater* **2015,** *3* (6), 813-820.
36. Kruk, S.; Kivshar, Y., Functional Meta-Optics and Nanophotonics Govern by Mie Resonances. *Acs Photonics* **2017,** *4* (11), 2638-2649.
37. Zhang, L.; Ding, J.; Zheng, H. Y.; An, S. S.; Lin, H. T.; Zheng, B. W.; Du, Q. Y.; Yin, G. F.; Michon, J.; Zhang, Y. F.; Fang, Z. R.; Shalaginov, M. Y.; Deng, L. J.; Gu, T.; Zhang, H. L.; Hu, J. J., Ultra-thin high-efficiency mid-infrared transmissive Huygens meta-optics. *Nat Commun* **2018,** *9*.
38. Zhou, Z. P.; Li, J. T.; Su, R. B.; Yao, B. M.; Fang, H. L.; Li, K. Z.; Zhou, L. D.; Liu, J.; Stellinga, D.; Reardon, C. P.; Krauss, T. F.; Wang, X. H., Efficient Silicon Metasurfaces for Visible Light. *Acs Photonics* **2017,** *4* (3), 544-551.
39. Wang, L.; Kruk, S.; Tang, H.; Li, T.; Kravchenko, I.; Neshev, D. N.; Kivshar, Y. S., Grayscale transparent metasurface holograms. *Optica* **2016,** *3* (12), 1504.
40. Zhao, W.; Jiang, H.; Liu, B.; Song, J.; Jiang, Y.; Tang, C.; Li, J., Dielectric Huygens' Metasurface for High-Efficiency Hologram Operating in Transmission Mode. *Sci Rep-Uk* **2016,** *6* (1), 30613.
41. Gigli, C.; Li, Q.; Chavel, P.; Leo, G.; Brongersma, M.; Lalanne, P., Fundamental limitations of Huygens metasurfaces for optical beam shaping. *arXiv pre-print server* **2020**.
42. Xiong, B.; Xu, Y.; Wang, J.; Li, L.; Deng, L.; Cheng, F.; Peng, R. W.; Wang, M.; Liu, Y., Realizing Colorful Holographic Mimicry by Metasurfaces. *Adv Mater* **2021,** *33* (21), 2005864.
43. Liu, H.; Yang, H.; Li, Y. R.; Song, B. X.; Wang, Y. F.; Liu, Z. R.; Peng, L.; Lim, H.; Yoon, J.; Wu, W., Switchable All-Dielectric Metasurfaces for Full-Color Reflective Display. *Adv Opt Mater* **2019,** *7* (8).
44. Shrestha, S.; Overvig, A. C.; Lu, M.; Stein, A.; Yu, N., Broadband achromatic dielectric metalenses. *Light Sci Appl* **2018,** *7*, 85.